International Journal of Biological Macromolecules 333 (2025) 148808

Contents lists available at ScienceDirect

International Journal of Biological Macromolecules

journal homepage: www.elsevier.com/locate/ijbiomac

Assembly dynamics and metabolic flux redistribution mediated by *accA1/accA2* functional divergence in *Streptomyces coelicolor*

Shiyu Wu [a,b,d], Ximing Chen [b,c,*], Yujie Wu [b,c], Xue Yu [b,c], Xiaomin Niu [b,c], Tuo Chen [a,b,**], Wei Zhang [b,c], Guangxiu Liu [b,c], Paul Dyson [e]

[a] State Key Laboratory of Cryospheric Science and Frozen Soil Engineering, Northwest Institute of Eco-Environment and Resources, Chinese Academy of Sciences, 730000, China
[b] Key Laboratory of Extreme Environmental Microbial Resources and Engineering of Gansu Province, Lanzhou, 730000, China
[c] Key Laboratory of Ecological Safety and Sustainable Development in Arid Lands, Northwest Institute of Eco-Environment and Resources, Chinese Academy of Sciences, Lanzhou, 730000, China
[d] University of Chinese Academy of Sciences, Beijing, 100049, China
[e] Institute of Life Science, Swansea University Medical School, Singleton Park, Swansea, SA2 8PP, UK

ARTICLE INFO

Keywords:
Streptomyces coelicolor
Acyl-CoA carboxylase complex
accA1/accA2
Genetic redundancy
Functional divergence
Metabolic reprogramming

ABSTRACT

The acyl-CoA carboxylase (YCC) complex catalyzes the first committed step in both fatty acid and polyketide biosynthesis and is therefore essential for primary and secondary metabolism in *Streptomyces*. In *Streptomyces coelicolor*, the YCC family comprises acetyl-CoA carboxylase (ACC) and propionyl-CoA carboxylase (PCC), which are homologous multi-subunit complexes sharing identical α subunits encoded by *accA1* and *accA2*. However, the functional divergence between these two α subunit genes remains unclear. In this study, we systematically characterized *accA1* and *accA2* in *S. coelicolor* M145 through expression profiling, physiological assays, metabolomics, and Co-IP analyses. qPCR and Western blot results revealed distinct expression patterns of the two genes. Overexpression of *accA2* promoted rapid biomass accumulation and enhanced primary metabolism, whereas *accA1* overexpression perturbed early primary metabolism and triggered premature and elevated actinorhodin production, indicating distinct physiological functions. Metabolomic profiling further supported the notion that *accA2* overexpression primarily activated primary metabolic pathways, whereas *accA1* overexpression strongly induced secondary metabolism. Co-IP assays demonstrated that AccA1 and AccA2 exhibit different assembly preferences: AccA2-containing complexes remained relatively stable, whereas AccA1 displayed higher flexibility and preferentially assembled into ACC complexes. Collectively, these findings reveal that *accA1* and *accA2* differentially regulate carbon flux through distinct expression dynamics and assembly preferences. AccA1 predominantly channels flux toward secondary metabolite biosynthesis, while AccA2 primarily supports fatty acid and other primary metabolic processes. This work provides a theoretical basis for optimizing metabolic engineering strategies in *Streptomyces*.

1. Introduction

Streptomyces is the type genus of the phylum Actinomycetota, renowned for its complex morphological differentiation cycle and extraordinarily diverse secondary metabolism [1,2]. *Streptomyces coelicolor* serves as a model organism for studying secondary metabolism, owing to its ability to synthesize a diverse range of natural products [3,4]. During secondary metabolite biosynthesis, acyl-CoA carboxylase (YCC) catalyzes the carboxylation of acetyl-CoA, propionyl-CoA, or long-chain acyl-CoA [5]. This enzyme plays central roles not only as initiators of fatty acid biosynthesis but also as key contributors to the production of polyketide antibiotics and other secondary metabolites

* Corresponding author at: Key Laboratory of Extreme Environmental Microbial Resources and Engineering of Gansu Province, Lanzhou 730000, China.
** Corresponding author at: State Key Laboratory of Cryospheric Science and Frozen Soil Engineering, Northwest Institute of Eco-Environment and Resources, Chinese Academy of Sciences, 730000, China.
E-mail addresses: wushiyu23@mails.ucas.ac.cn (S. Wu), chenximing@nieer.ac.cn (X. Chen), wuyujie18@mails.ucas.ac.cn (Y. Wu), yuxue@lzb.ac.cn (X. Yu), niuxiaomin22@mails.ucas.ac.cn (X. Niu), chentuo@lzb.ac.cn (T. Chen), ziaoshen@163.com (W. Zhang), liugx@lzb.ac.cn (G. Liu), p.j.dyson@swansea.ac.uk (P. Dyson).

https://doi.org/10.1016/j.ijbiomac.2025.148808
Received 19 August 2025; Received in revised form 24 October 2025; Accepted 4 November 2025
Available online 5 November 2025

[5–7]. Consequently, YCC has emerged as an important target for metabolic engineering aimed at modulating metabolic flux and optimizing biosynthetic pathways.

In *S. coelicolor*, the YCC family consists of two major complexes, acetyl-CoA carboxylase (ACC) and propionyl-CoA carboxylase (PCC) [8]. Each complex comprises a catalytic core formed by the α and β subunits, and an ε subunit that modulates their activity [9–13]. The α subunit forms carboxylated biotin and attaches it to the biotin carrier protein (BCCP) [7,14]. Meanwhile, the β subunit moves the carboxyl group from biotin-BCCP to the acyl-CoA substrate [7,14]. Gago et al. reported that these enzymes generally assemble as $\alpha_6\beta_6$ or $\alpha_2\beta_2$ holoenzymes [12]. Since the β subunit of *S. coelicolor* forms a hexameric structure [7], its YCC complex likely adopts an $\alpha_6\beta_6$ architecture, although the precise structural role of the ε subunit remains unresolved.

The ACC and PCC complexes of *S. coelicolor* share a common α subunit encoded by two nearly identical genes, *accA1* (Acetyl-coenzyme A carboxylase carboxyl transferase subunit alpha1; SCO6271) and *accA2* (Acetyl-coenzyme A carboxylase carboxyl transferase subunit alpha2; SCO4921), differing by only two nucleotides, yet producing α subunits with identical amino acid sequences, whereas their β (AccB or PccB) and ε (AccE or PccE) subunits are distinct [8,15]. The β subunit predominantly determines substrate specificity [7,16]: AccB can utilize acetyl-CoA, propionyl-CoA, and butyryl-CoA, whereas PccB accepts only propionyl-CoA and butyryl-CoA [7]. Disruption of *pccB* does not affect viability, suggesting its role in secondary metabolism [17], whereas *accB* deletion is lethal, underscoring its essential function in primary metabolism [9]. Interestingly, supplementation with long-chain fatty acids rescues the growth of the *accB* mutant but not the production of actinorhodin (ACT) or undecylprodigiosin (RED), indicating that *accB* also contributes to secondary metabolism [9]. While most engineering efforts have focused on modifying the β subunit to expand substrate range, the biological function of the α subunit has remained poorly understood. Its participation in multiple carboxylase complexes hints at a potential coordinating role in metabolic flux and resource allocation, yet systematic characterization of α-subunit function within the YCC complex has been lacking.

The α subunit of *S. coelicolor* YCC is encoded by *accA1* and *accA2*, representing a typical case of genetic redundancy [8,15,18]. This redundancy, coupled with the sharing of multiple complex subunits, suggests the existence of a synergistic mechanism that enhances functional robustness, enables dynamic resource allocation, and allows flexible metabolic regulation [19,20]. Such mechanisms enable fine-tuned adaptation to fluctuating environmental conditions. In *Saccharomyces cerevisiae*, for example, both the *CYC1* and *CYC7* genes encode cytochrome *c*, with *CYC1* being expressed at high oxygen concentrations and *CYC7* at low oxygen concentrations [21,22]. They share subunits to maintain electron transport in complexes III/IV [21]. In *Cycloclasticus pugetii* PS-1, six *rhd* subunit genes respond differentially to naphthalene concentrations: high concentrations activate *rhdPS1α/β*, while other *rhd* genes are upregulated at lower concentrations to maintain metabolic balance [23]. Studies have shown that *accA2* is essential for *S. coelicolor* viability, whereas *accA1* is dispensable [15]. This finding suggests that, despite encoding identical proteins, the two genes appear to have functionally diverged. However, their spatiotemporal expression patterns, regulatory mechanisms, and influence on metabolic flux remain largely unexplored.

This study aims to elucidate the functional divergence and regulatory roles of *accA1* and *accA2* in *S. coelicolor* M145. Time-course transcriptional profiling revealed that *accA1* exhibited a higher and more dynamic transcription level than *accA2*, and protein analysis during the exponential phase further confirmed its higher expression level. Overexpression experiments demonstrated that *accA2* facilitated primary metabolic processes and enhanced strain growth, whereas *accA1* suppressed early primary metabolism, significantly promoted secondary metabolism, and increased ACT yield by 24 %. Untargeted metabolomics further corroborated that the overexpression of *accA2* was predominantly engaged in primary metabolic pathways, whereas the overexpression of *accA1* facilitated secondary metabolic pathways. Co-IP assays revealed distinct subunit assembly preferences between the two α subunit proteins, showing that AccA2-containing complexes remained relatively stable under both native and overexpression conditions, whereas AccA1 exhibited greater variability and tended to assemble preferentially into ACC complexes.

2. Materials and methods

2.1. Strains, plasmids, and general techniques for DNA manipulations

All strains and plasmids used in the present study are listed in Table 1. *Escherichia coli* DH5α was used as the general cloning host. *E. coli* ET12567 [24] was used as a donor for intergenic conjugation of plasmids into *Streptomyces*. *S. coelicolor* M145 was grown at 30 °C in MS or R2YE medium. *E. coli* strains were grown in LB medium at 37 °C. Kanamycin (50 μg/mL), hygromycin B (50 μg/mL), or/and chloramphenicol (34 μg/mL) were added when necessary.

2.2. RNA extraction and qPCR experiment

Total RNAs were extracted from *S. coelicolor* M145 using RNA Extraction Kit (Tsingke, China). Reverse transcription amplification was performed using the SynScript®III RT SuperMix for qPCR (Tsingke, China). The cDNA product generated through reverse transcription was diluted 3-folds and utilized as a template for qPCR amplification using the ArtiCanCEO SYBR qPCR Mix (Tsingke, China). The *hrdB* gene was used as an internal control. The expression level of genes was calculated using the $2^{-\Delta\Delta Ct}$ method. All the primers used for qPCR above are shown in Table 2.

2.3. Western blot

Cells were lysed in Triton X-100 lysis buffer (20 mM Tris-HCl, 150 mM NaCl, 1 % Triton X-100, 10 % glycerol, 5 mM EDTA, 1 mM PMSF), disrupted by ultrasonication, and centrifuged (12,000 rpm, 20 min, 4 °C). Protein concentration in the supernatant was measured using a BCA assay. 50 μg of proteins per sample were separated by 12 % SDS-PAGE, transferred to PVDF membranes, blocked with skim milk for 2 h, and incubated overnight at 4 °C with anti-Flag and anti-HA antibodies. After washing, the membrane was incubated for 2 h at room temperature with HRP-conjugated goat anti-mouse secondary antibody. Protein bands were visualized using chemiluminescence, and band intensity was quantified using ImageJ software, with GAPDH used as the internal loading control [27].

2.4. Co-immunoprecipitation and mass spectrometry

Exponentially growing cells were harvested, resuspended in Triton X-100 lysis buffer, and lysed by ultrasonication. Protein concentrations were determined using the BCA assay. Protein interactions were carried out using Flag-tag Nanoab Magnetic Beads and control nanobody-conjugated beads (NuoyiBio, China), following the manufacturer's instructions. Samples were then analyzed by SDS-PAGE and silver staining [28,29], with remaining portions digested with trypsin at 37 °C for 16–18 h and subjected to LC-MS/MS.

2.4.1. Chromatographic conditions

The column used was a reversed-phase C18 column (0.15 × 150 mm, Column Technology Inc.). The mobile phase consisted of 0.1 % formic acid in water (A) and 0.1 % formic acid in 84 % acetonitrile (B), with gradient elution as follows: from 0 to 50 min, the proportion of B increased linearly from 4 % to 50 %; from 50 to 54 min, it further increased from 50 % to 100 %; and from 54 to 60 min, B was maintained at 100 %. The column was equilibrated with 95 % mobile phase A before

Table 1
Strains and plasmids used in this study.

Strains and plasmids	Genotype	Reference
Strains		
S. coelicolor strains		
M145	The parental strain	Bentley et al. [25]
SCO6271-1	M145 overexpressing *accA1*	This study
SCO4921-1	M145 overexpressing *accA2*	This study
M145/ pSH152	M145 containing the plasmid pSH152	This study
SCO6271-2	M145 overexpressing *accA1* with an N-terminal Flag tag	This study
SCO6271-3	M145 overexpressing *accA1* with a C-terminal Flag tag	This study
SCO4921-2	M145 overexpressing *accA2* with an N-terminal Flag tag	This study
SCO4921-3	M145 overexpressing *accA2* with a C-terminal Flag tag	This study
SCO6271-4	M145 carrying *accA1* under its native promoter with an N-terminal Flag tag	This study
SCO6271-5	M145 carrying *accA1* under its native promoter with a C-terminal Flag tag	This study
SCO4921-4	M145 carrying *accA2* under its native promoter with an N-terminal Flag tag	This study
SCO4921-5	M145 carrying *accA2* under its native promoter with a C-terminal Flag tag	This study
SCO4921-6	M145 carrying *accA2* under its native promoter with an N-terminal HA tag	This study
E. coli strains		
DH5α	F-*φ80lacZΔM15Δ(lacZYA-argF) U169recA1endA1hsdR17(rk-mk+) phoAsupE44λ-thi-1gyrA96relA1*	TransGen Biotech Co., LTD
ET12567/ pUZ8002	*dam-13*::Tn9 *dcm-6 hsdM*; containing the non-transmissible RP4 derivative plasmid pUZ8002	Flett et al. [24]
Plasmids		
pSH152	*E. coli-S. coelicolor* shuttle vector, hygromycin resistance	Mistry et al. [26]
pSH152-1	pSH152 containing *accA1* with *ermE** promoter	This study
pSH152-2	pSH152 containing *accA2* with *ermE** promoter	This study
pSH152-3	pSH152 carrying N-terminal Flag-tagged *accA1* driven by the *ermE** promoter.	This study
pSH152-4	pSH152 carrying C-terminal Flag-tagged *accA1* driven by the *ermE** promoter.	This study
pSH152-5	pSH152 carrying N-terminal Flag-tagged *accA2* driven by the *ermE** promoter.	This study
pSH152-6	pSH152 carrying C-terminal Flag-tagged *accA2* driven by the *ermE** promoter.	This study
pSH152-7	pSH152 carrying N-terminal HA-tagged *accA2* driven by the *ermE** promoter.	This study
pSH152-8	pSH152 carrying N-terminal Flag-tagged *accA1* driven by its native promoter.	This study
pSH152-9	pSH152 carrying C-terminal Flag-tagged *accA1* driven by its native promoter.	This study
pSH152-10	pSH152 carrying N-terminal Flag-tagged *accA2* driven by its native promoter.	This study
pSH152-11	pSH152 carrying C-terminal Flag-tagged *accA2* driven by its native promoter.	This study

Table 2
Primers used for this study.

Primer	Sequence (5′-3′)
accA1-F	GGTGATTACCGCGGGATGG
accA1-R	AGATTCTCCTCACTCACTCGATTAC
accA2-F	GGTACTACAAGGGCTTTCGGG
accA2-R	AAGCCGAGTTTAGGGACTGC
hrdB-F	GAAGCTGACCAGATTCCGGC
hrdB-R	TTCGCTGCGACGCTCTTTC

analysis. Samples were loaded via an autosampler onto ZORBAX 300SB-C18 peptide traps (Agilent Technologies, Wilmington, DE) before separation.

2.4.2. Mass spectrum conditions

Peptide digests were separated by capillary high-performance liquid chromatography and analyzed using a Q Exactive HF-X mass spectrometer (Thermo Fisher). The total analysis time was 60 min. Data were acquired in positive ion mode. Mass spectra were collected using a data-dependent acquisition method, in which each full MS scan was followed by MS/MS scans of the top 10 most intense precursor ions.

2.4.3. Data analysis

The raw data from the mass spectrometry experiments were extracted from the custom database (Supplementary Table 1) using MaxQuant 1.5.5.1 to facilitate protein identification and quantitative analysis.

2.5. LC/QTOF for untargeted metabolomics

2.5.1. Chromatographic conditions

The column used was ZORBAX Eclipse Plus C18 (2.1 × 50 mm, 1.8 μm). The mobile phase consisted of an aqueous 0.1 % formic acid solution (A) and methanol (B), with gradient elution as follows: from 0 to 1 min, the proportion of B increased from 10 % to 40 %; from 1 to 2.5 min, it further increased from 40 % to 65 %; from 2.5 to 5 min, it increased again from 65 % to 80 %; and finally, between 5 and 7.1 min, it remained at 80 %. The column temperature was maintained at 30 °C while the flow rate was set at 0.3 mL/min. The sample size injected was 2.0 μL.

2.5.2. Mass spectrum conditions

TIS ion source in positive ion mode detection was used with a gas curtain gas pressure of 35 psi (approximately equivalent to 6.895 kPa), atomizing gas pressure of 45 psi, and auxiliary gas pressure of 50 psi. The applied ion spray potential was 5000 V. The scanning time for mass spectrometry analysis was one second within a scanning range of m/z 50–2000.

2.5.3. Data analysis

The raw spectral data were processed and analyzed utilizing Mass-Hunter Explorer (Agilent), MetaboAnalyst (https://www.metaboanalyst.ca/), and Metware Cloud (https://cloud.metware.cn).

2.6. Dynamic detection of actinomycin (ACT) and undecylprodigiosin (RED)

ACT and RED were quantified as previously described with modifications [30,31]. *S. coelicolor* M145, SCO6271-1, and SCO4921-1 were cultured on R2YE and sampled at various time points. For ACT, samples were adjusted to pH 10 with KOH, incubated for 1 h at room temperature, centrifuged (12,000 rpm, 5 min), and absorbance measured at 640 nm. For RED, acidified methanol (pH 2) was incubated overnight, centrifuged, and measured at 530 nm. ACT and RED levels were expressed as OD_{640}/mg and OD_{530}/mg dry weight, respectively.

3. Results

3.1. accA1 and accA2 have a different pattern of expression

In *S. coelicolor* M145, *accA2* is essential for growth, whereas *accA1* is not [9,15]. Despite encoding the same α subunit, they appear to be subject to distinct regulatory controls. Thus, a time-course transcriptional analysis was conducted on *accA1* and *accA2*, which encode the α subunit of the YCC complex. Due to their high sequence similarity, primer design was guided by the 150 bp 5′-UTR regions of each gene, following the strategy of E. Rodríguez et al. [9]. Melting curve analysis

of qPCR confirmed primer specificity, allowing clear differentiation between *accA1* and *accA2* (Fig. S1).

Samples were collected at six time points (12 h, 24 h, 36 h, 48 h, 60 h, and 72 h) to encompass the lag phase, exponential phase, transition phase, and stationary phase of M145 growth cycle. Using *hrdB* as an internal reference, qPCR revealed that *accA1* transcript levels were approximately 6- to 8-fold higher than those of *accA2* ($p < 0.001$; Fig. 1A). The transcription level of *accA2* remained relatively stable throughout growth, whereas the transcription level of *accA1* increased slightly at 48 h and decreased thereafter (at 60 h and 72 h). Since *accA1* is non-essential [9,15], its relatively high transcription level may be attributed to differences in promoter activity and mRNA stability.

Because transcript abundance does not always correlate with protein level [32], we next assessed protein expression by Western blotting (WB) at 48 h (Fig. 1B and C). AccA1, tagged with a Flag epitope at either the N- or C-terminus, consistently appeared as a ~125 kDa band—approximately twice its predicted molecular weight—suggesting potential dimer formation. In contrast, HA-tagged AccA2 was detected at its theoretical molecular weight of ~62.5 kDa. Densitometric analysis of WB bands revealed no significant difference between N- and C-terminally tagged AccA1 variants; however, both exhibited protein levels approximately 2-fold higher than AccA2 ($p < 0.001$). Although overall protein levels were lower than corresponding transcript levels, the significantly higher abundance of AccA1 during the exponential phase indicates robust expression. Taken together, these results indicate that *accA1* and *accA2* are differentially regulated at both the transcriptional and translational levels.

3.2. Overexpression of accA1 or accA2 alters growth dynamics as well as antibiotic production

To further elucidate the functional roles of *accA1* and *accA2* in primary and secondary metabolism, overexpression strains were constructed in which *accA1* (SCO6271-1) or *accA2* (SCO4921-1) was driven by the constitutive *ermE** promoter. These strains were used to evaluate the effects of α-subunit overexpression on growth and antibiotic production (ACT and RED).

On both sporulation medium (MS) and fermentation medium (R2YE), the *accA1* overexpression strain exhibited a prolonged lag phase and slower initial growth compared with the wild-type strain M145 (Fig. 2A). Once entering the exponential phase, its growth rate increased, and biomass eventually surpassed that of M145 during the stationary phase. In contrast, the *accA2*-overexpressing strain showed a shortened lag phase, faster exponential growth, and higher overall biomass accumulation than both the wild type and the *accA1* overexpression strain. These results suggest that *accA2* overexpression enhances primary metabolic capacity, whereas *accA1* overexpression transiently suppresses primary metabolism during the early growth phase. However, this suppression appears to be relieved during exponential growth, leading to a moderate enhancement of biomass accumulation relative to M145. Although biomass was quantified by dry weight—a standard proxy for growth in *Streptomyces* [33,34]—we further corroborated these trends through colony morphology and sporulation patterns on solid media (Fig. S2), which consistently showed delayed development in the *accA1* overexpression strain and enhanced sporulation in *accA2*-overexpressing cells.

Quantitative analysis of time-course production of ACT and RED was performed using absorbance-based measurements (Figs. 2B and S3). Interestingly, overexpression of *accA1* and *accA2* had similar effects on the biosynthesis of the two pigmented antibiotics but with different magnitudes. Both mutant strains had a reduced RED production but an enhanced ACT production. The *accA1* overexpression strain showed a 24 % increase in ACT yield and initiated production earlier, whereas the *accA2* overexpression strain displayed only a modest 5 % enhancement.

Taken together, these findings suggest that constitutive expression of *accA1* perturbs early carbon flux, leading to a temporary suppression of primary metabolism and an extended lag phase. As cultures enter the exponential phase, this suppression is relieved, and the precocious activation of ACT biosynthesis indicates a metabolic shift toward secondary metabolism. In contrast, *accA2* overexpression promotes primary metabolic activity, supporting faster growth and sustained biomass accumulation.

3.3. Overexpression of accA1 or accA2 alters the composition of the metabolome differently

To assess the global metabolic consequences of *accA1* and *accA2* overexpression, untargeted LC-MS-based metabolomics was performed on the wild-type strain M145 and the corresponding overexpression strains (SCO6271-1 and SCO4921-1). Raw LC/Q-TOF data were processed using MassHunter Explorer, and principal component analysis (PCA) was conducted in MetaboAnalyst to visualize overall metabolic

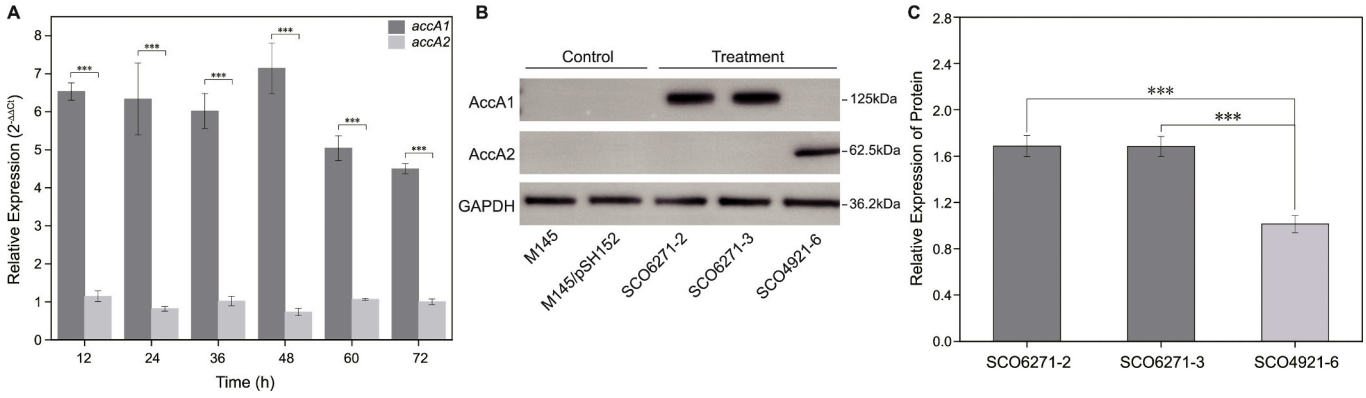

Fig. 1. Expression levels of *accA1* and *accA2* in wild-type M145 and overexpression strains. (A) Time-course qPCR analysis of *accA1* and *accA2* transcript levels in strain M145. *hrdB* was used as an internal reference gene. Dark gray bars, *accA1*; light gray bars, *accA2*. Bars represent mean values; error bars indicate standard deviations ($n = 3$). Statistical significance was assessed using Student's *t*-test (**$p < 0.001$). (B) WB analysis of AccA1 and AccA2 protein levels in total crude lysates from the strain M145, the strain M145 carrying the empty plasmid pSH152, and the overexpression strains. M145/pSH152, the strain M145 with empty plasmid pSH152; SCO6271-4, the strain carrying *accA1* under its native promoter with an N-terminal Flag tag; SCO6271-5, the strain carrying *accA1* under its native promoter with a C-terminal Flag tag; SCO4921-6, the strain carrying *accA2* under its native promoter with an N-terminal HA tag. AccA1 and AccA2 were detected using mouse anti-FLAG and anti-HA antibodies, respectively. GAPDH was used as the loading control. Blots shown are representative of three independent experiments. (C) Quantification of AccA1 and AccA2 protein levels normalized to GAPDH. Data are presented as mean ± standard deviation ($n = 3$). Statistical significance was determined by Student's *t*-test (**$p < 0.001$).

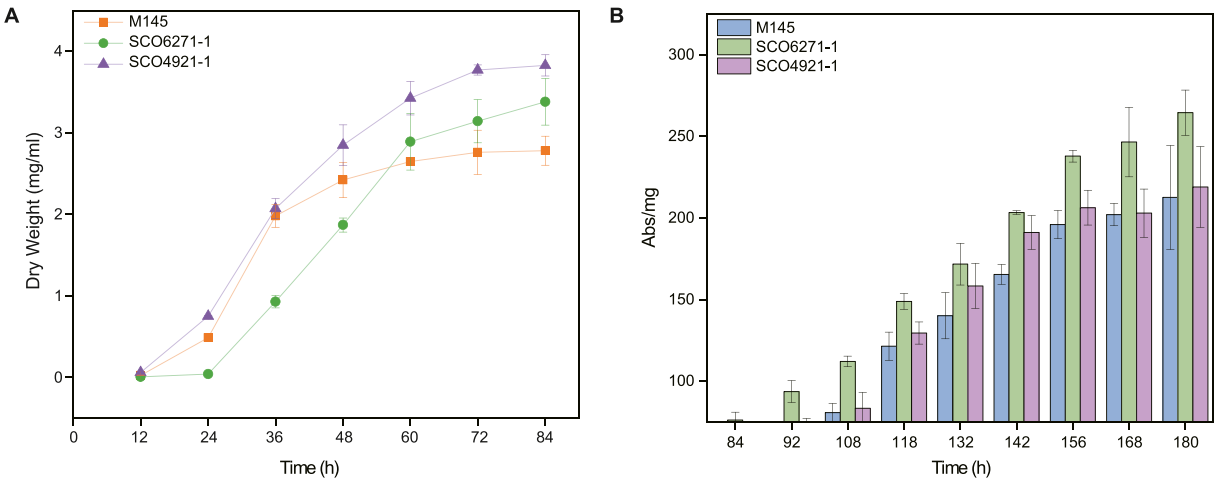

Fig. 2. Growth profiles and secondary metabolite production of wild-type M145 and *accA1/accA2* overexpression strains on R2YE media. (A) Growth curve of wild-type strain M145 and *accA1/accA2* overexpression strain in liquid R2YE medium. Orange square, strain M145; Green circle, *accA1* overexpression strain (SCO6271-1); Purple triangle, *accA2* overexpression strain (SCO4921-1). (B) Quantification of ACT production by strains M145 and *accA1/accA2*-overexpressing strains cultured in liquid R2YE medium. Blue, strain M145; Green, *accA1* overexpression strain (SCO46271-1); Pink, *accA2* overexpression strain (SCO4921-1). Data represent mean values from three biological replicates.

variation among strains.

The PCA score plot showed clear separation among the three groups, indicating that both *accA1* and *accA2* overexpression caused substantial metabolic reprogramming. Notably, the *accA1* overexpression strain exhibited the greatest divergence from M145 (Fig. 3A), suggesting that *accA1* has a stronger impact on global metabolism than *accA2*.

Differentially expressed metabolites (DEMs) were identified using thresholds of $|\log_2 FC| \geq 2$, VIP > 1, and $p < 0.05$. A total of 5314 DEMs were detected between M145 and the *accA1* overexpression strain (3784 upregulated and 1530 downregulated), 4721 between M145 and the *accA2* overexpression strain (3183 upregulated and 1538 downregulated), and 2316 between the two overexpression strains (1324 upregulated and 992 downregulated) (Fig. 3C; Supplementary Tables S3–S5).

KEGG pathway enrichment analysis further revealed distinct metabolic biases between the two overexpression strains. DEMs from the *accA1* overexpression strain versus M145 were enriched in 29 level-2 KEGG pathways, most prominently in biosynthesis of secondary metabolites, encompassing 515 DEMs (410 upregulated) (Fig. 3D; Supplementary Table 6). Additional enrichment occurred in lipid metabolism (322 upregulated), terpenoid and polyketide metabolism (67 upregulated), and microbial metabolism in diverse environments (134 upregulated), indicating a broad rerouting of carbon flux toward specialized metabolite production. In contrast, DEMs from the *accA2* overexpression strain versus M145 were enriched in 28 pathways, primarily in lipid metabolism (361 of 415 upregulated) and biosynthesis of secondary metabolites (303 of 401 upregulated) (Fig. 3D; Supplementary Table 7). Direct comparison between the two overexpression strains confirmed this divergence, with secondary metabolism-related metabolites constituting the largest proportion (19.1 %) of upregulated compounds in the *accA1* overexpression strain relative to the *accA2* overexpression strain (Fig. 3B).

Overall, these results indicate that *accA1* overexpression predominantly activates secondary metabolic pathways, whereas *accA2* overexpression mainly enhances primary metabolism.

3.4. Co-immunoprecipitation experiments revealed distinct assembly preferences of AccA1 and AccA2 with β and ε subunits

To investigate how AccA1 and AccA2 associate with the β and ε subunits of the ACC (AccB, AccE) and PCC (PccB, PccE) complexes, expression plasmids encoding either N- or C-terminally Flag-tagged variants of *accA1* and *accA2* were constructed. These were expressed under either their native promoters (P_{native}) or the constitutive *ermE** promoter to generate native-expression strains (SCO6271-4/5 and SCO4921-4/5) and overexpression strains (SCO6271-2/3 and SCO4921-2/3). After 48 h of cultivation, the immunoprecipitated complexes were visualized by silver staining (data not shown) and identified by LC–MS/MS (Supplementary Tables 1 and 2). Protein signal intensities were normalized by label-free quantification (LFQ) to generate heatmaps of relative abundance (Fig. 4A and S4). Relative binding ratios between each α subunit and its partner subunits were then calculated from the signal intensity ratio of the co-precipitated proteins to that of the corresponding α subunit (Fig. 4B; Supplementary Table 2). The Flag-tag position (N- vs C-terminal) had no detectable influence on Co-IP results, confirming that tag placement did not bias pull-down efficiency.

Under native expression conditions, both AccA1 and AccA2 exhibited comparable assembly ratios with the ACC-specific β subunit AccB, and these ratios were generally higher than those observed with the PCC β subunit PccB. However, the two α subunits displayed distinct preferences toward PccB: AccA1 showed a relatively weaker interaction, whereas AccA2 associated more strongly, suggesting that AccA2 is more prone to participate in PCC complex formation. For the ε subunit, only the ACC-specific AccE was detected, and AccA1 displayed a stronger interaction with AccE than AccA2. Given that the ε subunit is essential for ACC catalytic activity [8,12], the comparable AccA1/AccA2 binding to AccB but tighter association of AccA1 with AccE implies that ACC complexes containing AccA1 likely exhibit higher enzymatic activity than those formed with AccA2.

In the overexpression strains, *accA2* overexpression (SCO4921-2/3) did not markedly alter the relative assembly ratios of AccA2 with AccB, AccE, or PccB, consistent with its proposed role in maintaining basal metabolic functions. In contrast, *accA1* overexpression (SCO6271-2/3) led to substantial changes in subunit association patterns. AccA1 exhibited markedly enhanced interactions with both AccB and AccE compared with the native condition, indicating that *accA1* overexpression during the exponential phase strongly promotes ACC complex assembly. Conversely, the binding of AccA1 to PccB was significantly reduced upon *accA1* overexpression, suggesting that elevated AccA1 expression further limits its participation in PCC assembly. These results collectively support the notion that AccA1 preferentially drives ACC formation and thereby contributes to enhanced secondary metabolism, whereas AccA2 predominantly supports enzyme complexes assembly linked to primary metabolic processes.

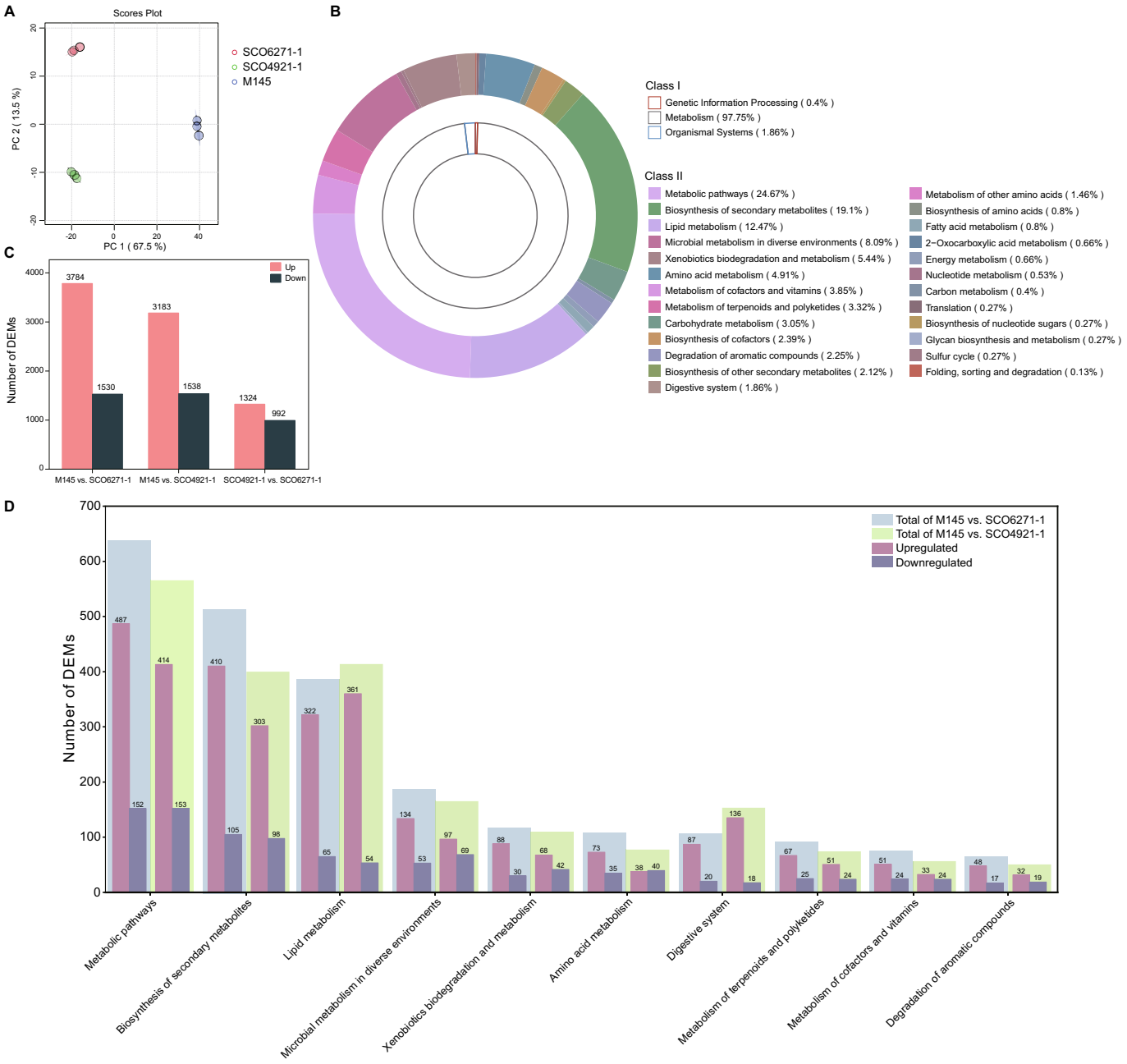

Fig. 3. Impact of *accA1* and *accA2* overexpression on secondary metabolism in *S. coelicolor* M145. (A) PCA of metabolomic profiles for the wild-type strain M145 and the *accA1* and *accA2* overexpression strains (SCO6271-1 and SCO4921-1). (B) Circular KEGG pathway enrichment plot of upregulated differential metabolites (DEMs) in strain SCO6271-1 and SCO4921-1. The inner ring displays the distribution of enriched pathways at KEGG level-1, while the outer ring illustrates pathway enrichment at KEGG level-2. The size of each segment indicates the relative proportion of pathways within each category. (C) Numbers of DEMs among M145, SCO6271-1, and SCO4921-1. Metabolites were selected based on VIP > 1, $|\log_2 FC| \geq 2$, and $p < 0.05$. (D) Composite bar charts showing KEGG pathway enrichment of DEMs between M145 vs. SCO6271-1, and M145 vs. SCO4921-1. The top 10 pathways are displayed based on the total number of enriched DEMs. For each pathway, the total number of DEMs is represented by the outer bar, with inner grouped bars indicating the number of upregulated and downregulated metabolites.

In summary, these findings indicate that AccA1 and AccA2 display distinct assembly preferences. AccA1 exhibits greater flexibility in complex formation, whereas AccA2 remains relatively stable. AccA1 preferentially assembles into ACC complexes and interacts more strongly with the ε subunit AccE, likely resulting in higher catalytic efficiency. Together with the preceding experimental observations, these results support a model in which AccA1-dominant ACC complexes channel carbon flux toward secondary metabolite biosynthesis, while AccA2-dominant complexes primarily sustain fatty acid and other primary metabolic pathways.

4. Discussion

The functional divergence of homologous genes often reflects an evolutionary strategy by which organisms develop redundancy and resource-sharing mechanisms to maintain metabolic robustness while enabling fine-tuned regulation [35–37]. In *S. coelicolor*, the α subunit of the YCC complex is encoded by two homologous genes, *accA1* and *accA2*. Here, we systematically dissected their distinct roles in metabolic regulation and demonstrated that these homologs jointly control the partitioning of carbon flux between primary and secondary metabolism through transcriptional regulation and differential complex assembly.

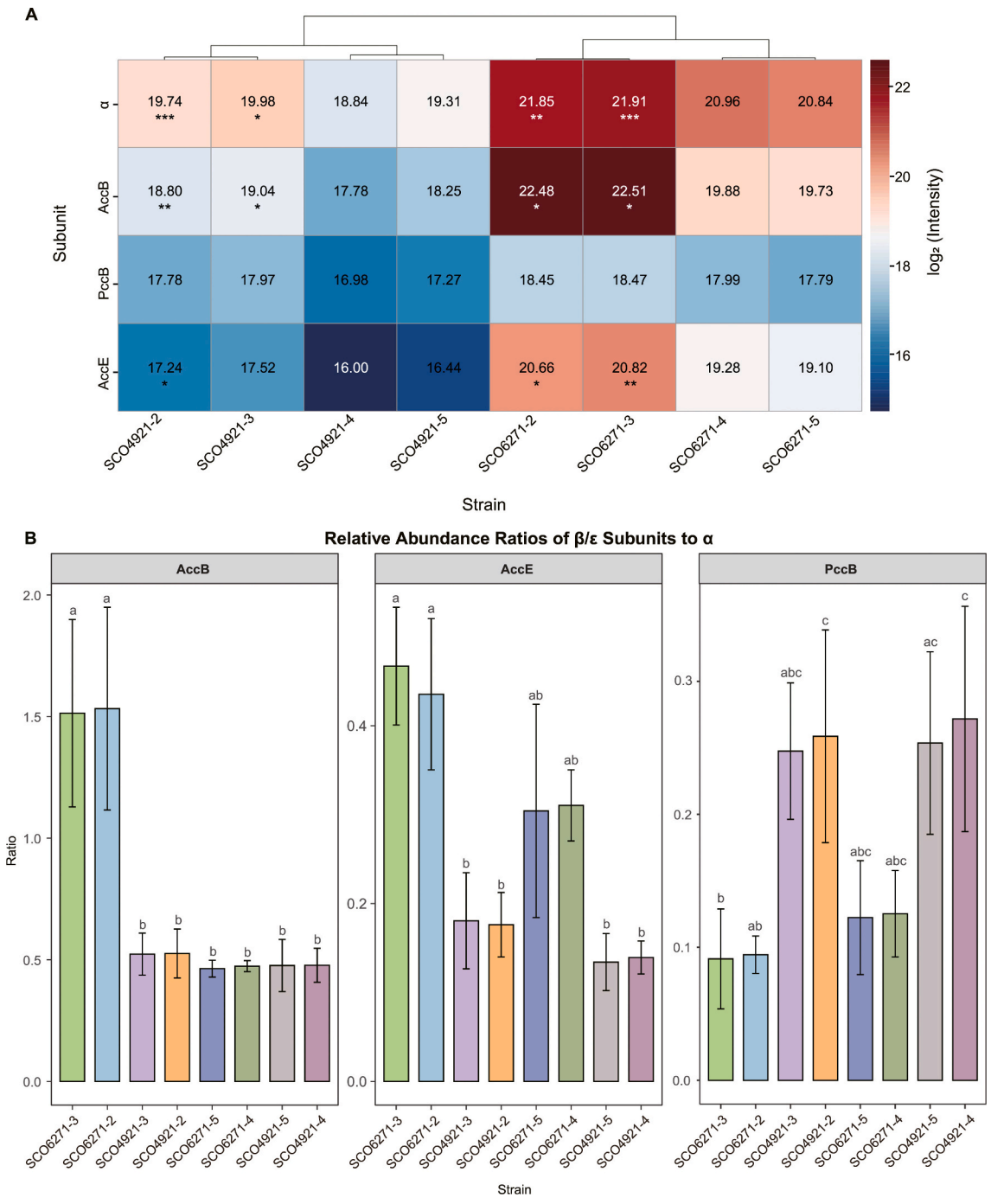

Fig. 4. Subunit binding ratios and relative protein abundances determined by Co-IP coupled with LC-MS/MS (A) Heatmap showing relative protein abundances of selected subunits. Color intensity reflects abundance levels, with red indicating higher abundance and blue indicating lower relative abundance. Numeric values represent log-transformed average relative protein abundance across three biological replicates. Asterisks indicate statistically significant differences between overexpression strains and their native controls based on unpaired *t*-tests (*$p < 0.05$, **$p < 0.01$, ***$p < 0.001$). The symbol "α" indicates AccA1 or AccA2 in the respective samples. SCO6271-2 and SCO6271-3 represent *accA1* overexpression strains tagged with N- or C-terminal Flag. SCO6271-4 and SCO6271-5 indicate strains expressing *accA1* under its native promoter with N- or C-terminal Flag tags. SCO4921-2 and SCO4921-3 refer to *accA2* overexpression strains with N- or C-terminal Flag tags. SCO4921-3 and SCO4921-4 represent strains expressing *accA2* under its native promoter with N- or C-terminal Flag tags. (B) Relative signal intensity ratios of β or ε subunits to AccA1 or AccA2, defined as the ratio of the signal strength of each relevant subunit to that of AccA1 or AccA2. Each bar represents the ratio of the respective subunit signal intensity to that of AccA1 or AccA2 across the eight strains. Subunits are grouped as follows: β subunit of the ACC complex (AccB group), ε subunit of the ACC complex (AccE group), and β subunit of the PCC complex (PccB group). Data represent mean values from three biological replicates; error bars indicate standard error (SE). Lowercase letters above bars indicate statistically significant differences among groups (Tukey's HSD test, $p < 0.05$). Groups sharing the same letter are not significantly different; groups labeled with different letters are significantly different. Groups labeled with multiple letters are not significantly different from any group indicated by those letters.

Our results reveal that *accA2* primarily supports primary metabolism, whereas *accA1* predominantly contributes to secondary metabolism.

Previous studies reported that the deletion of *accA1* had only minor effects on growth and antibiotic production [9,15], leading to the assumption that it functions in the synthesis of a specific or unknown polyketide compound [38]. In contrast, we found that *accA1* overexpression significantly reshaped the global metabolic state and enhanced ACT accumulation (Figs. 2B and 3), a product previously thought to be unrelated to its function. This finding indicates that *accA1* exerts a broader influence on cellular metabolism rather than being confined to a single biosynthetic pathway. Conversely, deletion of *accA2* caused severe growth defects [9,15], suggesting that despite encoding identical proteins, the two genes have undergone functional specialization. Such "redundant but nonequivalent" partitioning of homologous genes is common in eukaryotes (e.g., GLUT transporters or GhCIPK6 homologs [39,40]) but remains rare among prokaryotes [41]. Given the highly complex metabolic and developmental networks in *Streptomyces* [42], this divergence likely represents an adaptive strategy to balance robustness with regulatory flexibility during metabolic transitions.

Both AccA1 and AccA2 can assemble with AccB/E to form the ACC complex—a central metabolic hub linking primary and secondary metabolism [9]. Their distinct physiological roles thus likely arise from differences in the composition and regulatory dynamics of the resulting complexes. The qPCR analysis showed that *accA1* transcription was consistently higher than *accA2* throughout the growth cycle, reaching up to an 8-fold difference in the late exponential phase (~48 h, Fig. 1A). However, the corresponding protein levels differed by only about 2-fold (Fig. 1B and C), suggesting partial decoupling between transcription and translation. In contrast, *accA2* transcription remained relatively constant, consistent with its constitutive role in primary metabolism. We therefore propose that during early growth, ACC complexes predominantly consist of AccA2 and AccB to sustain fatty acid biosynthesis and other primary metabolic activities, whereas *accA1* expression remains low. As the culture enters the metabolic transition phase (~48 h), *accA1* expression rises sharply, potentially triggering the onset of secondary metabolism. Interestingly, constitutive *accA1* overexpression prolonged the lag phase (Fig. 2A), implying that premature production of AccA1 sequesters AccB from primary metabolism, thereby reducing the formation of primary-type ACC complexes. Subsequently, as AccB expression increased markedly during the exponential phase, metabolomic analysis showed reactivation of lipid metabolism pathways, restoring normal growth(Figs. 2A, 4A, S2, and S4). These results suggest that elevated AccB expression compensates for the metabolic imbalance caused by *accA1* overexpression. Altogether, our findings support a model in which AccA2-containing complexes mainly sustain primary metabolism, whereas AccA1-containing complexes facilitate the transition toward secondary metabolism. However, since dynamic data on YCC complex assembly and subunit interactions throughout the growth cycle are still lacking, the detailed regulatory mechanism warrants further investigation.

Co-IP analysis revealed clear differences in assembly behavior between AccA1 and AccA2. In the *accA2* overexpression strain, the subunit ratios remained essentially constant (Fig. 4B), indicating that AccA2 primarily serves to stabilize the structure of the primary-type ACC complex. Moreover, the total amount of precipitated protein increased (Figs. 4A and S4), which is in line with the higher biomass observed in this strain (Fig. 2A). In contrast, *accA1* overexpression significantly altered subunit composition: its affinity for AccB/E increased, whereas interaction with PccB decreased, suggesting preferential participation in ACC complex formation—a pattern consistent with its role in secondary metabolism regulation. No PccE signal was detected, likely due to its low abundance or stage-specific expression; its precise function within the PCC complex remains to be clarified.

Metabolite profiling further supported this interpretation. Overexpression of *accA1* and *accA2* increased ACT production by 24 % and 5 %, respectively, demonstrating that enhancing α subunit expression within the YCC complex effectively promotes polyketide biosynthesis. In addition to metabolic redistribution, oxidative stress has been reported to act as an important signal that triggers ACT and other polyketide biosynthesis in *Streptomyces* [43–45]. Although oxidative stress was not directly assessed in this study, it may represent an additional factor contributing to the enhanced ACT production observed upon *accA1* overexpression. Because polyketide production depends on the precise coordination between primary and secondary metabolism, direct metabolic interventions often yield limited improvement due to an imbalance between these processes [46]. The regulatory pattern revealed here suggests that α subunit overexpression promotes ACC complex assembly, increases precursor availability, and facilitates the metabolic transition from growth to production phase. This mechanistically simple yet robust regulation may provide an efficient strategy for optimizing polyketide synthesis at the systems level. Importantly, the three-subunit YCC complex is highly conserved across *Streptomyces* species (data not shown), implying that α subunit engineering could represent a generalizable approach for improving polyketide yields.

Conversely, RED biosynthesis was markedly suppressed in both overexpression strains (Fig. S2). RED formation depends on malonyl-CoA, L-proline, and acetyl-CoA as key precursors [47,48]. The enhanced ACT accumulation and enzyme complex assembly patterns suggest that malonyl-CoA is unlikely to be limiting. Moreover, metabolomic analysis revealed that *accA2* overexpression elevated intracellular L-proline levels, whereas *accA1* overexpression caused no significant change (Supplementary Table 4), indicating that reduced RED production was not due to proline limitation. Previous studies showed that ACC and RedP (3-oxoacyl-[ACP] synthase) compete for acetyl-CoA as a substrate [47,49,50]. Therefore, we propose that α-subunit overexpression increases ACC complex abundance, intensifying the carboxylation of acetyl-CoA and consequently reducing its availability for RED biosynthesis.

In conclusion, our study elucidates the functional divergence of *accA1* and *accA2* in coordinating primary and secondary metabolism in *S. coelicolor*. The two homologs differ in transcriptional dynamics, complex assembly preferences, and metabolic consequences, underscoring their complementary roles in redistributing carbon flux during metabolic transitions. These insights deepen our understanding of YCC complex regulation and highlight α-subunit engineering as a promising and broadly applicable strategy to enhance polyketide production in *Streptomyces*.

CRediT authorship contribution statement

Shiyu Wu: Writing – original draft, Visualization, Software, Methodology, Investigation, Formal analysis, Data curation. **Ximing Chen:** Writing – review & editing, Funding acquisition, Conceptualization. **Yujie Wu:** Methodology, Investigation. **Xue Yu:** Visualization. **Xiaomin Niu:** Investigation. **Tuo Chen:** Writing – review & editing, Supervision. **Wei Zhang:** Supervision, Funding acquisition. **Guangxiu Liu:** Supervision, Funding acquisition. **Paul Dyson:** Writing – review & editing.

Declaration of competing interest

The authors have declared that no conflict of interest exists.

Acknowledgements

We sincerely thank Key Laboratory of Extreme Environmental Microbial Resources and Engineering of Gansu Province for providing facilities and support for experiments. This work was financially supported by Scientific Project of Gansu Province (22ZD6WA035), West Light Foundation of the Chinese Academy of Sciences (xbzg-zdsys-202105), and the National Natural Science Foundation of China (U22A20451).

Appendix A. Supplementary data

Supplementary data to this article can be found online at https://doi.org/10.1016/j.ijbiomac.2025.148808.

Data availability

I have shared the link to my data at the Attach File step.

References

[1] K. Flärdh, M.J. Buttner, *Streptomyces* morphogenetics: dissecting differentiation in a filamentous bacterium, Nat. Rev. Microbiol. 7 (1) (2009) 36–49.
[2] Z. Zhou, J. Gu, Y. Li, Y. Wang, Genome plasticity and systems evolution in *Streptomyces*, BMC Bioinformatics 13 (Suppl. 10) (2012) S8.
[3] T. Dulermo, C. Lejeune, E. Aybeke, S. Abreu, J. Bleton, M. David, A. Deniset-Besseau, P. Chaminade, A. Thibessard, P. Leblond, M.-J. Virolle, Genome analysis of a variant of *Streptomyces coelicolor* M145 with high lipid content and poor ability to synthetize antibiotics, Microorganisms 11 (6) (2023) 1470.
[4] P.A. Hoskisson, G.P.v. Wezel, Streptomyces coelicolor, Trends Microbiol. 27 (5) (2019) 468–469.
[5] L. Tong, Structure and function of biotin-dependent carboxylases, Cell. Mol. Life Sci. 70 (5) (2013) 863–891.
[6] T. Robbins, Y.-C. Liu, D.E. Cane, C. Khosla, Structure and mechanism of assembly line polyketide synthases, Curr. Opin. Struct. Biol. 41 (2016) 10–18.
[7] A. Arabolaza, M.E. Shillito, T.-W. Lin, L. Diacovich, M. Melgar, H. Pham, D. Amick, H. Gramajo, S.-C. Tsai, Crystal structures and mutational analyses of acyl-CoA carboxylase beta subunit of *Streptomyces coelicolor*, Biochemistry 49 (34) (2010) 7367–7376.
[8] L. Diacovich, S. Peirú, D. Kurth, E. Rodríguez, F. Podestá, C. Khosla, H. Gramajo, Kinetic and structural analysis of a new group of acyl-CoA carboxylases found in *Streptomyces coelicolor* A3(2), J. Biol. Chem. 277 (34) (2002) 31228–31236.
[9] E. Rodríguez, C. Banchio, L. Diacovich, M.J. Bibb, H. Gramajo, Role of an essential acyl coenzyme A carboxylase in the primary and secondary metabolism of *Streptomyces coelicolor* A3(2), Appl. Environ. Microbiol. 67 (9) (2001) 4166–4176.
[10] D.G. Kurth, G.M. Gago, A.d.l. Iglesia, B.B. Lyonnet, T.-W. Lin, H.R. Morbidoni, S.-C. Tsai, H. Gramajo, ACCase 6 is the essential acetyl-CoA carboxylase involved in fatty acid and mycolic acid biosynthesis in mycobacteria, Microbiology 155 (8) (2009) 2664–2675.
[11] G. Gago, D. Kurth, L. Diacovich, S.-C. Tsai, H. Gramajo, Biochemical and structural characterization of an essential acyl coenzyme A carboxylase from *Mycobacterium tuberculosis*, J. Bacteriol. 188 (2) (2006) 477–486.
[12] G. Gago, L. Diacovich, A. Arabolaza, S.-C. Tsai, H. Gramajo, Fatty acid biosynthesis in actinomycetes, FEMS Microbiol. Rev. 35 (3) (2011) 475–497.
[13] T.H. Tran, Y.-S. Hsiao, J. Jo, C.-Y. Chou, L.E.P. Dietrich, T. Walz, L. Tong, Structure and function of a single-chain, multi-domain long-chain acyl-CoA carboxylase, Nature 518 (7537) (2014) 120–124.
[14] K.-K. Shivaiah, B. Upton, B.J. Nikolau, Kinetic, structural, and mutational analysis of acyl-CoA carboxylase from *Thermobifida fusca* YX, Front. Mol. Biosci. 7 (2021) 615614.
[15] E.R. Guez, H. Gramajo, Genetic and biochemical characterization of the alpha and beta components of a propionyl-CoA carboxylase complex of *Streptomyces coelicolor* A3(2), Microbiology (Reading) 145 (Pt 11) (1999) 3109–3119.
[16] L. Diacovich, D.L. Mitchell, H. Pham, G. Gago, M.M. Melgar, C. Khosla, H. Gramajo, S.-C. Tsai, Crystal structure of the beta-subunit of acyl-CoA carboxylase: structure-based engineering of substrate specificity, Biochemistry 43 (44) (2004) 14027–14036.
[17] A.V. Demirev, A. Khanal, B.R. Sedai, S.K. Lim, M.K. Na, D.H. Nam, The role of acyl-coenzyme A carboxylase complex in lipstatin biosynthesis of *Streptomyces toxytricini*, Appl. Microbiol. Biotechnol. 87 (3) (2010) 1129–1139.
[18] Á.J. Láruson, S. Yeaman, K.E. Lotterhos, The importance of genetic redundancy in evolution, Trends Ecol. Evol. 35 (9) (2020) 809–822.
[19] J. Masel, M.L. Siegal, Robustness: mechanisms and consequences, Trends Genet. 25 (9) (2009) 395–403.
[20] B.J. Strober, R. Elorbany, K. Rhodes, N. Krishnan, K. Tayeb, A. Battle, Y. Gilad, Dynamic genetic regulation of gene expression during cellular differentiation, Science 364 (6447) (2019) 1287–1290.
[21] T.M. Laz, D.F. Pietras, F. Sherman, Differential regulation of the duplicated isocytochrome c genes in yeast, Proc. Natl. Acad. Sci. USA 81 (14) (1984) 4475–4479.
[22] P.V. Burke, D.C. Raitt, L.A. Allen, E.A. Kellogg, R.O. Poyton, Effects of oxygen concentration on the expression of cytochrome c and cytochrome c oxidase genes in yeast, J. Biol. Chem. 272 (23) (1997) 14705–14712.
[23] A.L. Vogel, K.J. Thompson, D. Straub, F. Musat, T. Gutierrez, S. Kleindienst, Genetic redundancy in the naphthalene-degradation pathway of *Cycloclasticus pugetii* strain PS-1 enables response to varying substrate concentrations, FEMS Microbiol. Ecol. 100 (6) (2024) fiae060.
[24] F. Flett, V. Mersinias, C.P. Smith, High efficiency intergeneric conjugal transfer of plasmid DNA from Escherichia coli to methyl DNA-restricting *streptomycetes*, FEMS Microbiol. Lett. 155 (2) (1997) 223–229.
[25] S.D. Bentley, K.F. Chater, A.-M. Cerdeño-Tárraga, G.L. Challis, N.R. Thomson, K. D. James, D.E. Harris, M.A. Quail, H. Kieser, D. Harper, A. Bateman, S. Brown, G. Chandra, C.W. Chen, M. Collins, A. Cronin, A. Fraser, A. Goble, J. Hidalgo, T. Hornsby, S. Howarth, C.-H. Huang, T. Kieser, L. Larke, L. Murphy, K. Oliver, S. O'Neil, E. Rabbinowitsch, M.-A. Rajandream, K. Rutherford, S. Rutter, K. Seeger, D. Saunders, S. Sharp, R. Squares, S. Squares, K. Taylor, T. Warren, A. Wietzorrek, J. Woodward, B.G. Barrell, J. Parkhill, D.A. Hopwood, Complete genome sequence of the model actinomycete *Streptomyces coelicolor* A3(2), Nature 417 (6885) (2002) 141–147.
[26] B.V. Mistry, R.D. Sol, C. Wright, K. Findlay, P. Dyson, FtsW is a dispensable cell division protein required for Z-ring stabilization during sporulation septation in *Streptomyces coelicolor*, J. Bacteriol. 190 (16) (2008) 5555–5566.
[27] Y. Wu, M. Wu, G. He, X. Zhang, W. Li, Y. Gao, Z. Li, Z. Wang, C. Zhang, Glyceraldehyde-3-phosphate dehydrogenase: a universal internal control for Western blots in prokaryotic and eukaryotic cells, Anal. Biochem. 423 (1) (2012) 15–22.
[28] U.K. Laemmli, Cleavage of structural proteins during the assembly of the head of bacteriophage T4, Nature 227 (5259) (1970) 680–685.
[29] N. Berndt, R. Bergmann, C. Arndt, S. Koristka, M. Bachmann, Silver staining techniques of polyacrylamide gels, Methods Mol. Biol. 2018 (1853) 47–52.
[30] P. Liu, H. Zhu, G. Zheng, W. Jiang, Y. Lu, Metabolic engineering of *Streptomyces coelicolor* for enhanced prodigiosins (RED) production, Sci. China Life Sci. 60 (9) (2017) 948–957.
[31] Z. Yu, H. Zhu, F. Dang, W. Zhang, Z. Qin, S. Yang, H. Tan, Y. Lu, W. Jiang, Differential regulation of antibiotic biosynthesis by DraR-K, a novel two-component system in *Streptomyces coelicolor*, Mol. Microbiol. 85 (3) (2012) 535–556.
[32] T. Tebaldi, A. Re, G. Viero, I. Pegoretti, A. Passerini, E. Blanzieri, A. Quattrone, Widespread uncoupling between transcriptome and translatome variations after a stimulus in mammalian cells, BMC Genomics 13 (2012) 220.
[33] M. Fischer, R.G. Sawers, A universally applicable and rapid method for measuring the growth of *streptomyces* and other filamentous microorganisms by methylene blue adsorption-desorption, Appl. Environ. Microbiol. 79 (14) (2013) 4499–4502.
[34] T.H. Flowers, W. ST, Measurement of growth rates of *Streptomycetes*: comparison of turbidimetric and gravimetric techniques, J. Gen. Microbiol. 98 (1) (1977) 285–289.
[35] B. Conrad, S.E. Antonarakis, Gene duplication: a drive for phenotypic diversity and cause of human disease, Annu. Rev. Genomics Hum. Genet. 8 (2007) 17–35.
[36] J. Peng, Gene redundancy and gene compensation: an updated view, J. Genet. Genomics 46 (7) (2019) 329–333.
[37] P. Hunter, Understanding redundancy and resilience: redundancy in life is provided by distributing functions across networks rather than back-up systems: redundancy in life is provided by distributing functions across networks rather than back-up systems, EMBO Rep. 23 (3) (2022) e54742.
[38] C. Gao, D. Hindra, C. Mulder, M.A. Elliot Yin, Crp is a global regulator of antibiotic production in *Streptomyces*, mBio 3 (6) (2012).
[39] M. Mueckler, B. Thorens, The SLC2 (GLUT) family of membrane transporters, Mol. Asp. Med. 34 (2–3) (2013) 121–138.
[40] W. Sun, L. Xia, J. Deng, S. Sun, D. Yue, J. You, M. Wang, S. Jin, L. Zhu, K. Lindsey, X. Zhang, X. Yang, Evolution and subfunctionalization of CIPK6 homologous genes in regulating cotton drought resistance, Nat. Commun. 15 (1) (2024) 5733.
[41] D.C. Krakauer, J.B. Plotkin, Redundancy, antiredundancy, and the robustness of genomes, Proc. Natl. Acad. Sci. USA 99 (3) (2002) 1405–1409.
[42] O.S. Mohite, T.S. Jørgensen, T.J. Booth, P. Charusanti, P.V. Phaneuf, T. Weber, B. O. Palsson, Pangenome mining of the *Streptomyces* genus redefines species' biosynthetic potential, Genome Biol. 26 (1) (2025) 9.
[43] R. Dela Cruz, Y. Gao, S. Penumetcha, R. Sheplock, K. Weng, M. Chander, Expression of the *Streptomyces coelicolor* SoxR regulon is intimately linked with actinorhodin production, J. Bacteriol. 192 (24) (2010) 6428–6438.
[44] C. Esnault, T. Dulermo, A. Smirnov, A. Askora, M. David, A. Deniset-Besseau, I. B. Holland, M.J. Virolle, Strong antibiotic production is correlated with highly active oxidative metabolism in *Streptomyces coelicolor* M145, Sci. Rep. 7 (1) (2017) 200.
[45] X. Liu, J. Tang, L. Wang, R. Liu, Mechanism of CuO nano-particles on stimulating production of actinorhodin in Streptomyces coelicolor by transcriptional analysis, Sci. Rep. 9 (1) (2019) 11253.
[46] X. Chen, X.Y. Li, G.L. Zhang, C. Wang, L. C, Application of synthetic biology to the biosynthesis of polyketides, Synth. Biol. Eng. 2 (3) (2024) 10012.
[47] R. Singh, S. Mo, G. Florova, K.A. Reynolds, *Streptomyces coelicolor* RedP and FabH enzymes, initiating undecylprodiginine and fatty acid biosynthesis, exhibit distinct acyl-CoA and malonyl-acyl carrier protein substrate specificities, FEMS Microbiol. Lett. 328 (1) (2012) 32–38.
[48] M.G. Thomas, M.D. Burkart, C.T. Walsh, Conversion of L-proline to pyrrolyl-2-carboxyl-S-PCP during undecylprodigiosin and pyoluteorin biosynthesis, Chem. Biol. 9 (2) (2002) 171–184.
[49] S. Mo, B.S. Kim, K.A. Reynolds, Production of branched-chain alkylprodiginines in *S. coelicolor* by replacement of the 3-ketoacyl ACP synthase III initiation enzyme, RedP, Chem. Biol. 12 (2) (2005) 191–200.
[50] S. Mo, P.K. Sydor, C. Corre, M.M. Alhamadsheh, A.E. Stanley, S.W. Haynes, L. Song, K.A. Reynolds, G.L. Challis, Elucidation of the Streptomyces coelicolor pathway to 2-undecylpyrrole, a key intermediate in undecylprodiginine and streptorubin B biosynthesis, Chem. Biol. 15 (2) (2008) 137–148.